Dalton Transactions

PAPER

View Article Online
View Journal | View Issue

Cite this: *Dalton Trans.*, 2017, **46**, 16294

Crystal structures and magnetic properties of two series of phenoxo-*O* bridged dinuclear Ln_2 (Ln = Gd, Tb, Dy) complexes†

Marek Machata, Radovan Herchel, Ivan Nemec and Zdeněk Trávníček *

Received 14th September 2017,
Accepted 1st November 2017

DOI: 10.1039/c7dt03441e

rsc.li/dalton

Six dinuclear lanthanide compounds of the formulae $[Ln_2(3m\text{-}L4)_2(L2)_2(MeOH)_2]\cdot 6MeOH$ (Ln = Gd – **1a**, Tb – **1b**, and Dy – **1c**) and $[Ln_2(3m\text{-}L4)_2(L2)_2(DMF)_2]$ (Ln = Gd – **2a**, Tb – **2b**, and Dy – **2c**; DMF = *N*,*N*-dimethylformamide, $H_2$3m-L4 = (2-[(*E*)-(3-methoxysalicylidene)amino]phenol), and HL2 = 1,3-diphenyl-1,3-diketopropane) were prepared and characterized by elemental analysis, FTIR spectroscopy, thermogravimetric measurements, single-crystal X-ray structural analysis, and magnetometry, and Gd_2 and Dy_2 compounds by *ab initio* methods as well. The structural analysis revealed the isostructurallity of the compounds within the series of **1a–c** and **2a–c**. The analysis of the variable temperature magnetic data showed the presence of a weak antiferromagnetic coupling in the Gd_2 compounds (J/cm^{-1} = −0.13 for **1a** and J/cm^{-1} = −0.17 for **2a**). The magnetocaloric effect was studied on compound **2a** with the maximum value of $-\Delta S_M$ = 22.9 J kg^{-1} K^{-1} at T = 2.0 K and B = 9 T, which is the highest value among the Gd_2 double phenoxo-bridged compounds observed up to now. Both the Dy_2 compounds (**1c** and **2c**) exhibit slow-relaxation of magnetization in zero external static magnetic field. Magnetic anisotropy, intradimer magnetic coupling and magnetization blocking barriers were also studied by *ab initio* methods for **1c** and **2c**.

Introduction

Lanthanide-based coordination compounds have attracted increasing interest because of their potential applications as luminescent materials,[1] catalysts,[2] contrast agents in magnetic resonance imaging,[3] and molecular magnetic coolers,[4] and due to their capability to exhibit slow relaxation of magnetization of molecular origin with potential applications in quantum computing[5] and molecular spintronics.[6] The last mentioned property refers to a special class of molecular magnetic compounds, so called single molecule magnets (SMMs),[7] which exhibit slow relaxation of magnetization due to the presence of an intrinsic barrier of spin reversal (U_{eff}). This barrier occurs due to the presence of non-negligible magnetic anisotropy on the magnetic centres in the molecules. Lanthanide complexes have become good candidates for SMM preparation, because most of them have a large unquenched orbital momentum causing significant magnetic anisotropy of the metal center.[8] Furthermore, when considering polynuclear compounds, it should be noted that in 4f compounds the magnetic coupling between the metal centers is usually very weak. In other words, the magnetic properties of the 4f compounds are dominantly governed by the magnetic anisotropy of the ground term.[8] The main negative phenomenon influencing the dynamic magnetic properties of SMMs is fast quantum tunnelling of magnetization (QTM). This may arise from the transverse component of magnetic anisotropy[9] and/or magnetic dipolar intermolecular interactions.[10] The intermolecular interactions can be suppressed by careful design of the complex molecule and/or magnetic dilution of the sample, as tuning of the magnetic anisotropy is a more complicated task. There are several factors which determine the character of the magnetic anisotropy in lanthanide complexes such as the coordination number,[9b] the symmetry of the coordination polyhedron[11] and its distortion from the ideal symmetry,[11a,b] and the homogeneity of the electrostatic potential of the ligand field.[9a,b,12] Zero-field QTM can also be effectively suppressed by intramolecular exchange coupling in polynuclear compounds[13] despite the fact that the coupling between lanthanide atoms is weak.

Due to the spin-parity effect, most of the reported 4f based SMMs contain Dy^{III} atoms.[7d,14] Depending upon the nuclearity, the ligand field strength and the symmetry of the coordination polyhedron, Dy^{III} SMMs with a large U_{eff} have been reported[15a–c] over 800 K.[15d–f] In order to better understand the

Department of Inorganic Chemistry, Regional Centre of Advanced Technologies and Materials, Faculty of Science, Palacký University, 17. listopadu 12, CZ-771 46 Olomouc, Czech Republic. E-mail: zdenek.travnicek@upol.cz

† Electronic supplementary information (ESI) available. CCDC 1574217–1574222. For ESI and crystallographic data in CIF or other electronic format see DOI: 10.1039/c7dt03441e

magnetism of polynuclear Dy^{III} based SMMs, dinuclear Dy_2^{III} systems have been extensively studied as the simplest example.[7d] In the design of Dy_2^{III} based SMMs with a large U_{eff}, the right choice of differently charged ligands forming a heteroleptic coordination sphere turned out to be an even more important factor than the symmetry of the ligand field.[9a,b,12,16] One of the successful approaches for the preparation of such compounds is to react the negatively charged N,O-donor phenolate-based ligand L^{n-} with the dysprosium salt forming thus the $\{Dy_2L_2\}^{m+}$ unit, which might be further ligated by simple inorganic anions and/or solvent molecules.[13a,b,17] The utilization of tetradentate Schiff base ligands arising from the condensation of *o*-vanillin with aromatic amino alcohols has proved to be one of the ways to prepare such compounds.[17a,b] This type of tetradentate Schiff base ligand provides two distinct coordination pockets ensuring thus the coordination of two metal centres simultaneously, which are often coupled feromagnetically.[13a,17a,b] Small ligand changes (*e.g.* different conformations or substitutions of the main and/or auxiliary ligands) result in different coordination environments and thus they can influence the relaxation dynamics.[17b] It is noteworthy that these compounds often possess an inversion centre and therefore, there is just one symmetry independent magnetic centre in the molecule. This also means that local anisotropic axes are then aligned collinearly.[17c,f]

Apart from the SMM oriented research of lanthanide compounds, another active area of scientific research is devoted to molecular magnetic coolants. These are materials mostly based on Gd^{III} coordination compounds exhibiting the magnetocaloric effect (MCE).[18] The choice of Gd^{III}-based compounds is based on their small magnetic anisotropy and large spin (S = 7/2). Furthermore, a weak superexchange interaction usually present in polynuclear Gd-compounds results in the presence of low-lying excited (almost degenerate) spin states, which are desirable in order to achieve a larger MCE.[19]

In this work we report on the crystal structures of two new series of Ln_2^{III} complexes with the general formulae $[Ln_2^{III}(3m\text{-}L4)_2(L2)_2(MeOH)_2]\cdot 6MeOH$ (Ln = Gd, Tb, and Dy – **1a–c**) and $[Ln_2^{III}(3m\text{-}L4)_2(L2)_2(DMF)_2]$ (Ln = Gd, Tb, and Dy – **2a–c**), where DMF = *N*,*N*-dimethylformamide, $H_2$3m-L4 = (2-[(*E*)-(3-metoxysalicylidene)amino]phenol) and HL2 = 1,3-diphenyl-1,3-diketopropane. Their static and dynamic magnetic properties were studied thoroughly by experimental and theoretical methods. Furthermore, MCE was studied for compound **2a**. Finally, it must be noted that during the preparation of this report the structure and static and dynamic magnetic properties of **2c** were reported.[20] Nevertheless, herein we report on the detailed analysis of the relaxation processes in **2c** incorporating multiple relaxation pathways.

Results and discussion

Synthesis

Two isostructural Ln_2^{III} series **1a–c** and **2a–c** were prepared by the reaction of the tetradentate Schiff base ligand $H_2$3m-L4 and the bidentate β-diketone ligand HL2 with the corresponding Ln^{III} nitrate (Ln = Gd – **1a**, **2a**, Tb – **1b**, **2b** and Dy – **1c**, **2c**) in the presence of Pr_3N (tripropylammine) base in a molar ratio of 1 : 1 : 1 : 3 (Fig. 1). The main difference in the preparation of **1a–c** and **2a–c** series is in the used reaction solvents: compounds **1a–c** were prepared by using MeOH only, while **2a–c** were synthesized in a MeOH/DMF mixture (20 : 1 v : v). In **1a–c**, the MeOH molecules are found to be in both the molecular and crystal structures, whereas in **2a–c** only the DMF molecules are found to be coordinating directly the metal atoms (*vide infra*).

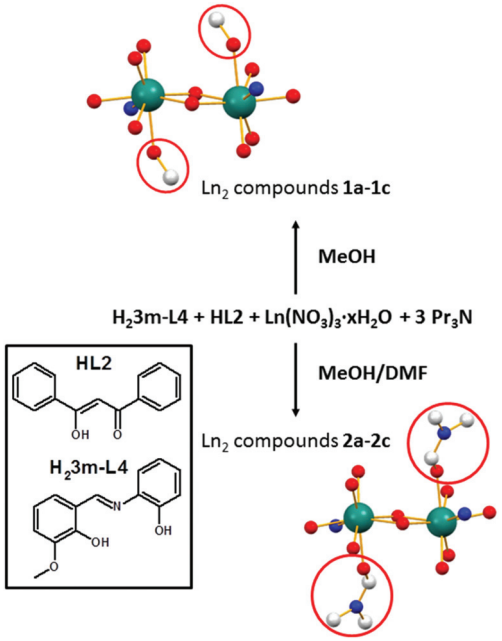

Fig. 1 Scheme of the synthesis of **1a–c** and **2a–c** with the depicted solvent molecules incorporated into the molecular structures.

Structure description

The tetradentate Schiff base ligand $H_2$3m-L4 provides four donor atoms for coordination to a central metal atom, *i.e.* two phenolate oxygen atoms (O_{Ph}) after its deprotonation, one methoxy oxygen (O_M) and one imino nitrogen atom (N_{Im}). In mononuclear complexes, the dianionic form of the ligand coordinates to the central atom using its N_{Im} and two O_{Ph} atoms (a tridentate coordination pocket, $\{NO_2\}$).[21] In polynuclear complexes, all of the donor atoms are involved in coordination in a way that the tridentate $\{NO_2\}$ pocket is formed again and one O_M together with one O_{Ph} atom (the $\{O_2\}$ donor atom set) forms the second bridging arrangement.[21b,22]

The utilization of the $H_2$3m-L4 ligand in the synthesis of metal complexes led to the preparation of polynuclear homometallic transition (Ni_4^{II}) and inner transition metal (Dy_4^{III}, U_2^{VI}) coordination compounds.[22d,e,23] More often, the preparations of the heterometallic 3d–4f ($Fe_2^{III}Ln^{III}$, $Mn_2^{III}Ln_2^{III}$, $Co_2^{II}Ln_2^{III}$,

$Ni^{II}_2Ln^{III}_2$, $Ni^{II}_4Ln^{III}_2$ and $Ni^{II}_8Dy^{III}_6$) coordination compounds were reported.[21b,22a–c,f–i]

The basic crystallographic and refinement data for **1a–c** and **2a–c** are listed in Table S1,† and selected distances and angles for the compounds are summarized in Table 1. The crystal structures of the presented compounds are composed of dinuclear complex molecules with the general formula $[Ln_2(3m\text{-}L4)_2(L2)_2(solv)_2]$, where solv = MeOH for **1a–c** and DMF for **2a–c**, and in the case of **1a–c**, additional six lattice MeOH molecules are found. In compounds **1a–c** and **2a–c**, the $H_2$3m-L4 ligand binds the Ln atoms in the same way as described above, *i.e.* one metal centre is coordinated by the $\{NO_2\}$ coordination pocket and simultaneously the same ligand coordinates the second Ln atom by the second $\{O_2\}$ coordination pocket. In this way, a centrosymmetric dimer with the $\{Ln_2O_2\}^{4+}$ core is formed (Fig. 2) and the $H_2$3m-L4 ligand occupies five coordination sites on each Ln atom. The additional three coordination sites are occupied by the deprotonated bidentate ketoenol and monodentate solvent ligands making thus the heteroleptic coordination sphere of octacoordinate central atoms.

The bond distances (Table 1) in **1a–c** and **2a–c** are shorter for the Ln–O_{Ph} and Ln–O_K (2.29–2.34 Å) than for Ln–O_M, Ln–N_{Im} and Ln–O_S bonds (2.39–2.54 Å). It should be noted that the Ln–O_S bonds are considerably shorter in **2a–c** than in **1a–c** (2.46–2.49 Å in **1a–c** and 2.39–2.43 Å in **2a–c**). The shape of the coordination polyhedron in all the compounds was determined by the SHAPE algorithm[24] to be a biaugmented trigonal prism (J50) with a significantly smaller distortion from the ideal shape found for **2a–c** (4.07–4.16 for **1a–c** and 2.13–2.31 for **2a–c**).

The phenolate oxygen atoms (O_{Ph}) mediate covalent bridging between the metal centres within the $\{Ln_2O_2\}^{4+}$ core with the averaged Ln–O_{Ph} distances (in Å) ranging from 2.35 to 2.37 (**1a–c**) and from 2.36 to 2.39 (**2a–c**). The corresponding Ln–O_{Ph}–Ln bonding angles adopt slightly different values

Table 1 Selected distances (in Å) and angles (°) for compounds **1a–c** and **2a–c**

	1a	1b	1c	2a	2b	2c
Ln–O_{Ph}[a]	2.339	2.325	2.313	2.338	2.329	2.312
Ln–O_M	2.5135(15)	2.5022(13)	2.4896(13)	2.503(3)	2.495(3)	2.4766(19)
Ln–N_{Im}	2.5055(19)	2.4893(17)	2.4791(17)	2.542(3)	2.523(3)	2.508(2)
Ln–O_K[b]	2.313	2.301	2.287	2.337	2.324	2.308
Ln–O_S	2.4913(15)	2.4705(13)	2.4587(14)	2.433(3)	2.413(3)	2.3936(19)
Ln–O_{Ph}–Ln	108.06(6)	108.38(5)	108.54(5)	106.28(10)	106.48(9)	106.97(7)
Ln···Ln[c]	3.8387(3)	3.8248(3)	3.8086(3)	3.8151(5)	3.8055(5)	3.7858(4)
Ln···Ln[d]	10.9275(5)[e] 14.0157(9)[f]	10.8918(4)[e] 14.0147(5)[f]	10.8879(4)[e] 14.0196(5)[f]	8.9439(9)	8.9239(5)	8.9039(5)

O_{Ph} – phenolate oxygen atom, O_M – methoxy oxygen atom, N_{Im} – imino nitrogen atom, O_K – β-ketoenolate oxygen atom, O_S – solvent oxygen atom, O_{S1}, O_{S2}, O_{S3} – intermolecular solvent oxygen atoms. [a] Averaged value for three Ln–O_{Ph} bond lengths. [b] Averaged value for two Ln–O_K bond lengths. [c] Intramolecular distances. [d] Intermolecular distances. [e] Within the 1D supramolecular chain. [f] Between the 1D supramolecular chains.

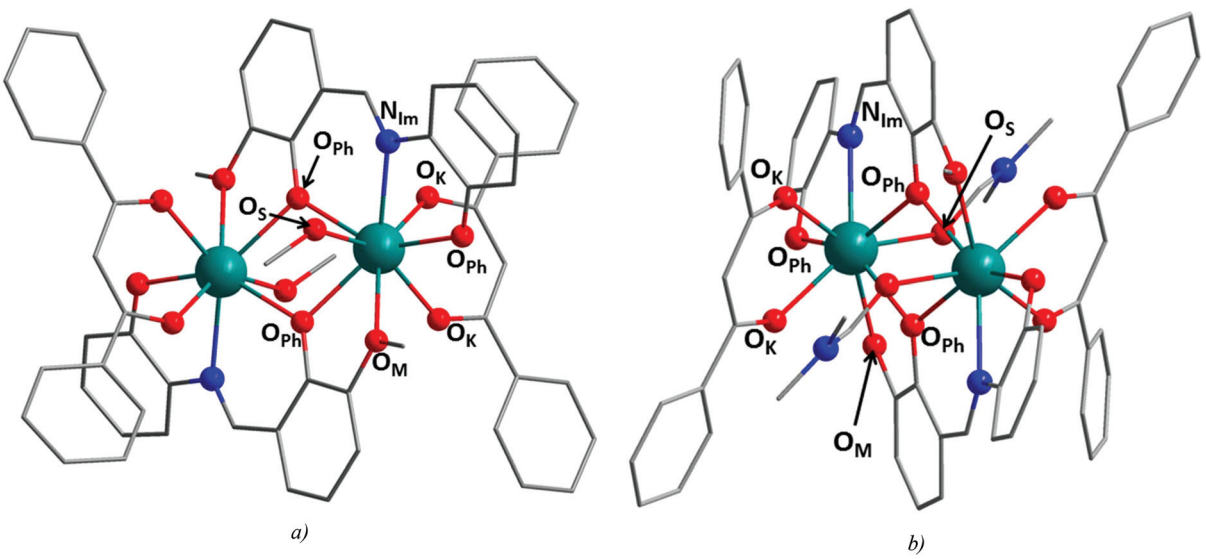

Fig. 2 Molecular structures of **1c** (a) and **2c** (b) with depicted coordination polyhedra of the corresponding central atoms. Hydrogen atoms are omitted for clarity. Colour code: Green (Dy), red (O), blue (N), and grey (C).

(108.1–108.5° in **1a–c** and 106.3–107.0° in **2a–c**). The intradimer Ln···Ln distances are slightly longer in **1a–c** (3.81–3.84 Å) than in **2a–c** (3.79–3.82 Å).

The crystal packing in **1a–c** significantly differs from that in **2a–c**. The adjacent dinuclear complex molecules of **1a–c** are connected through two symmetrically related (inversion centre) chains of the hydrogen bonds (Fig. 3, black dashed lines), which assemble the complex molecules into 1D arrays. Each supramolecular chain consists of one coordinated and three lattice MeOH molecules, which are interconnected by the O_S–H···O_S hydrogen bonding. On the end of the chain the MeOH molecule forms hydrogen bonds with the phenolate oxygen atoms of the coordinated Schiff base ligand. All the inchain O–H···O hydrogen bonds are rather short with the donor–acceptor distances ranging from 2.66 to 2.73 Å. Next important intermolecular interactions interconnect the neighbouring arrays of the complex molecules by the π–π stacking of the ketoenol aromatic rings with the distances between the centroids in the range of 3.63–3.66 Å for **1a–c**. The intermolecular in-chain Ln···Ln distances are in the range of 10.89–10.93 Å. The crystal structures of **2a–c** contain only weak C–H···π, C–H···O non-covalent interactions and these will not be described in greater detail. The closest intermolecular Ln···Ln distances range from 8.90 to 8.97 Å.

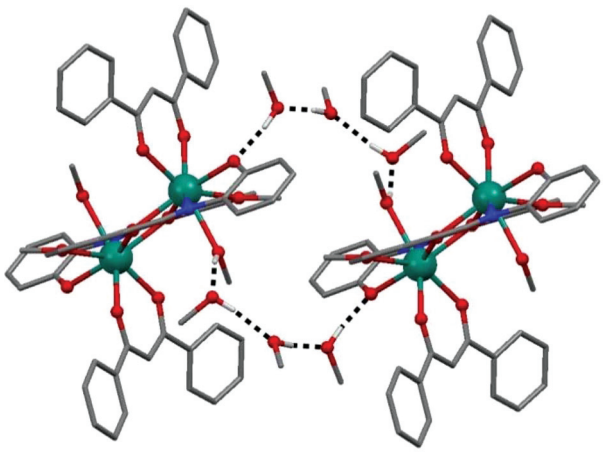

Fig. 3 Part of the crystal structure of **1c** with highlighted intermolecular hydrogen bonds (dashed black lines). Hydrogen atoms are omitted for clarity except for those which are included into hydrogen bonding. Colour code: Green (Dy), red (O), blue (N), grey (C), and dark grey (H).

Magnetic properties

Variable temperature DC magnetic measurements for compounds **1a–c** and **2a–c** are shown in Fig. 4. High temperature data are similar for all the compounds and are constant in the temperature region of 300–100 K with the μ_{eff}/μ_B values of 11.2 (**1a**), 13.8 (**1b**), 15.5 (**1c**), 11.4 (**2a**), 13.8 (**2b**), and 15.3 (**2c**) at 300 K which are close to the spin only values for such systems (Gd_2 – 11.2, $J = S = 7/2$, $g_J = 2$; Tb_2 – 13.8, $J = 6$, $g_J = 3/2$ Dy_2 – 15.1, $J = 15/2$, $g_J = 4/3$). The μ_{eff}/μ_B values for Gd_2 compounds remain constant down to approximately 50 K and then decrease to 8.4 and 8.0 at 1.9 K for **1a**, and **2a**, respectively. Low temperature magnetic data for the Tb_2 compounds show a gradual decrease with cooling and below 20 K, the μ_{eff}/μ_B values drop sharply to 11.6 and 11.5 at 1.9 K for **1b**, and **2b**, respectively. The μ_{eff}/μ_B *vs.* T data for **1c** follow the trend observed for the Tb_2 compounds but with a slight increase of μ_{eff}/μ_B below 20 K reaching 14.8 at 1.9 K. Variable temperature magnetic data for **2c** display a constant trend down to approximately 25 K followed by a sudden increase to 17.1μ_B at 1.9 K. The low temperature magnetic behaviour of all the compounds can be attributed to the depopulation of the excited Stark levels as well as magnetic anisotropy and/or antiferromagnetic magnetic interactions for the Gd_2 and Tb_2 compounds and ferromagnetic interactions in the Dy_2 compounds which seems to be stronger for **2c**. With regard to the smaller Dy···Dy distances for **2c** (3.8086(2) Å and 3.7858(4) Å for **1c** and **2c**, respectively), the observation of the stronger coupling for **2c** was expected.

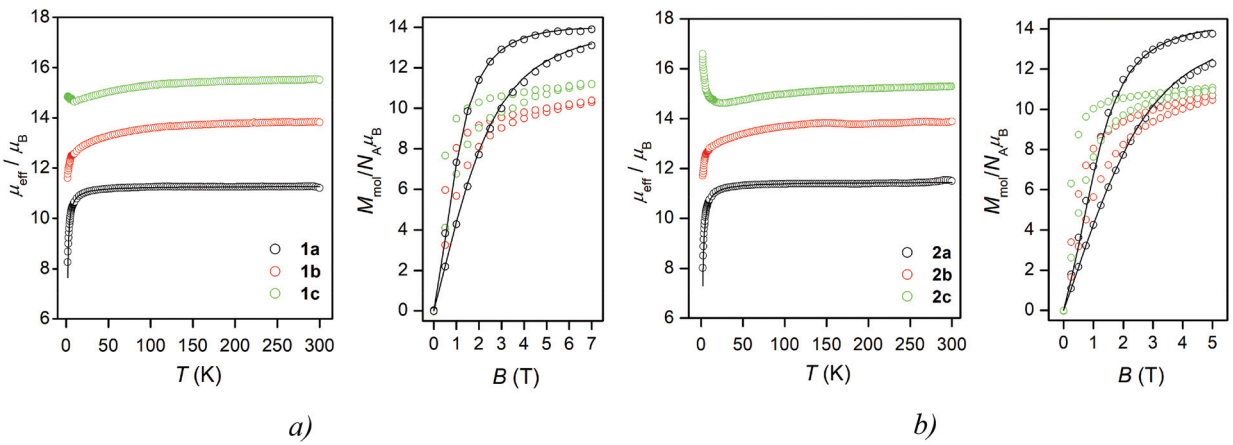

Fig. 4 Variable temperature magnetic measurements recorded under a DC magnetic field of 0.1 T and variable field magnetic measurements showed as $M_{mol}/N_A\mu_B$ *vs.* B dependence at 2 and 5 K for **1a–c** (a) and **2a–c** (b).

Field dependent DC magnetization data measured at 2 and 5 K (Fig. 4) display saturation of the molar magnetization to the expected value of 14 for the Gd_2 compounds. The magnetization for the Tb_2 and Dy_2 compounds does not saturate even at the highest applied fields (10.0, 10.7, 11.0 and 10.7 at 2 K for **1b**, **2b**, **1c**, and **2c**, respectively) that can be attributed to the presence of low lying excited states and/or magnetic anisotropy. A rapid increase of magnetization at low magnetic fields for the Dy_2 compounds is consistent with ferromagnetic interactions. There have been several reported examples of phenolato bridged Dy_2 compounds with ferromagnetic coupling.[14b,17a,25]

Variable temperature and field DC magnetic data for the Gd_2 compounds were fitted using the spin Hamiltonian approach using the formula

$$\hat{H} = -J(\vec{S}_1 \cdot \vec{S}_2) + \sum_{i=1}^{2} D_i\left(\hat{S}_z^2 + \hat{S}^2/3\right) + \mu_B B_a \sum_{i=1}^{2} g_a \hat{S}_a \qquad (1)$$

giving the following parameter values: J/cm^{-1} = –0.130(6), D/cm^{-1} = –0.22(4), and g = 2.009(3) (**1a**) and J/cm^{-1} = –0.17(1), D/cm^{-1} = –0.25(6), and g = 2.041(7) (**2a**).[26] The intradimer interactions J are similar for both compounds according to the expectations based on comparable separations between the metal centres (3.8387(3) Å and 3.8150(5) Å for **1a**, and **2a**, respectively). Also, the obtained values of constant J for **1a** and **2a** are in good agreement with similar Gd_2 compounds with double phenoxo bridges.[17c,f,27]

AC susceptibility measurements were performed for the Tb_2 (**1b** and **2b**) and Dy_2 (**1c** and **2c**) compounds. In the case of Tb_2 compounds, no out-of-phase AC susceptibility signal was observed at zero or non-zero static magnetic field. In contrast, both Dy_2 compounds exhibited a non-zero out-of-phase AC susceptibility signal already at zero static magnetic field (Fig. 5). The frequency dependence of the χ'' curves of both **1c** and **2c** indicates a slow relaxation of magnetization of molecular origin typical of SMMs. However, well-defined maxima on χ'' susceptibility were observed only for **2c**.

Thus, the temperature-dependent experimental data for **2c** were possible to analyse with the one-component Debye model ($\omega = 2\pi f$) as

$$\chi(\omega) = \chi_S + (\chi_T - \chi_S)/[1 + (i\omega\tau)^{1-\alpha}] \qquad (2)$$

providing values of isothermal (χ_T) and adiabatic (χ_S) susceptibilities, relaxation times (τ) and distribution parameters (α) – Fig. 5 and Table S2.† This enabled us to construct the Argand (Cole–Cole) plot displayed in Fig. 5. The temperature dependence of the relaxation times was analysed with eqn (3)

$$\frac{1}{\tau} = \frac{1}{\tau_{qt}} + CT^9 + \frac{1}{\tau_0}\exp(-U/kT) \qquad (3)$$

where quantum tunnelling, and Raman and Orbach relaxation processes were included. As a result, we obtained τ_{qt} = 1.18 × 10^{-3} s, C = 0.0222 K^{-9} s^{-1}, τ_0 = 5.07 × 10^{-13} and U = 169 K (Fig. 5). The value of U = 169 K is close to the energy of the first excited Kramers doublet, Δ = 223 K, calculated by CASSCF (*vide infra*), however much larger than those values reported for similar compounds in the literature (Table 2), which can be explained by the fact that only one relaxation process was included in their analyses.

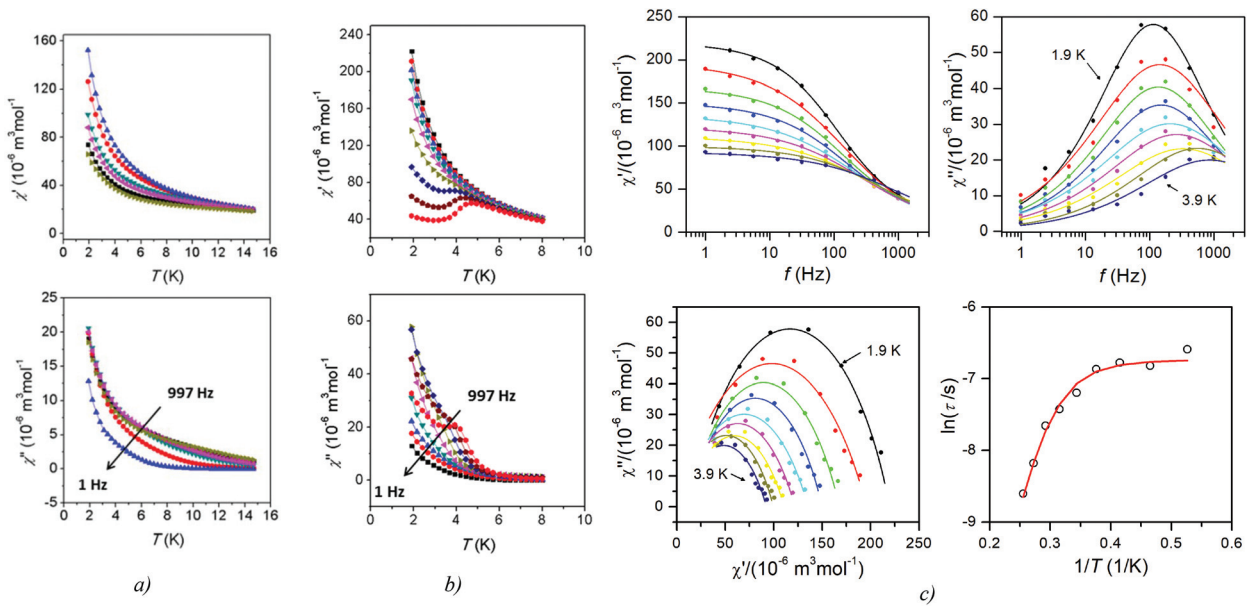

Fig. 5 (a–b) Frequency dependent ac susceptibility data recorded in zero DC magnetic field for compound **1c** (a) and **2c** (b). (c) AC susceptibility data for the Dy^{III} complex **2c** at the zero applied external field B_{DC} = 0.0 T. Top: Frequency dependence of χ' and χ'' molar susceptibilities. Full points – experimental data, full lines – fitted data using eqn (2). Bottom: Argand (Cole–Cole) plot and fit of the resulting relaxation times to eqn (3) (red line).

Table 2 List of the basic SMM characteristics of **1c**, **2c**, and five selected and previously reported octacoordinated compounds involving the $\{Dy_2L_2\}^{2+}$ units in their molecular structures. All the compounds are zero-field SMMs

Compound	τ_0 (s)	U (K)	Ref.
2c	5.07×10^{-13}	169	This work
$[Dy_2(salaph)_2(NO_3)_2(DMF)_2]$	4.4×10^{-7}(LTB)[a] 3.0×10^{-6} (HTB)[b]	11 (LTB)[a] 12 (HTB)[b]	17*f*
$[Dy_2(Hsalhap)_2(PhCOO)_2(MeOH)_2]$	2.1×10^{-7}	45	17*e*
$[Dy_2(ovinh)_2(NO_3)_2(MeOH)_2]$	3×10^{-7}	56	17*a*
$[Dy_2(ovpch)_2(NO_3)_2(H_2O)_2]\cdot 2H_2O$	5.3×10^{-7}	69	17*b*
$[Dy_2(napch)_2(NO_3)_2(MeOH)_2]\cdot 4MeCN$	1.9×10^{-6}	41	17*d*

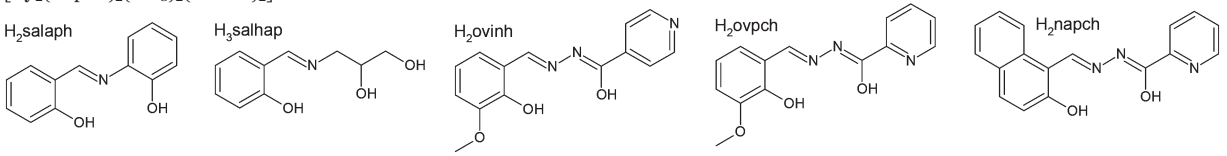

[a] Low temperature behaviour. [b] High temperature behaviour, H_2salaph = 2-{(*E*)-[(2-hydroxyphenyl)imino]methyl}phenol, H_3salhap = 3-{[(*E*)-(2-hydroxyphenyl)methylidene]amino}propane-1,2-diol, H_2ovinh = *N*-[(*E*)-(2-hydroxy-3-methoxyphenyl)methylidene]pyridine-4-carbohydrazonic acid, H_2ovpch = *N*-[(*E*)-(2-hydroxy-3-methoxyphenyl)methylidene]pyridine-2-carbohydrazonic acid, H_2napch = *N*-[(*E*)-(2-hydroxynaphthalen-1-yl)methylidene]pyridine-2-carbohydrazonic acid.

Magnetocaloric properties

With the aim to evaluate the magnetocaloric effect of the herein reported class of Gd^{III} compounds, the magnetization data were measured densely between 1.9 and 10.1 K in various magnetic fields up to 9 T for **2a** – Fig. 6. After that, the Maxwell equation

$$\left(\frac{dS}{dB}\right)_T = \left(\frac{dM}{dT}\right)_B \quad (4)$$

was used to evaluate the magnetocaloric effect as[28]

$$\Delta S_M(T_0, B) = \int_0^B \left(\frac{dM}{dT}\right)_B dB \quad (5)$$

The maximal value of $-\Delta S_M$ = 22.9 J kg^{-1} K^{-1} for **2a** was found at T = 2.0 K and B = 9 T (Fig. 6). This value is higher than 14.9–20.7 J kg^{-1} K^{-1} for other similar double phenoxo-bridged Gd_2 compounds.[27c,e,29] Recently, we reported on a general relationship for the magnetocaloric effect of Gd^{III} compounds, and two relationships were derived, $-\Delta S_M = 8914 \times (M_r/N(Gd))^{-0.913}$ and $-\Delta S_M = 39.5 c_m(Gd)^{0.364}$, based on the content of gadolinium expressed either as a relative molecular mass divided by the number of Gd atoms or by a mass concentration ($c_m = w_{Gd} \times \rho$).[30] Then, the estimated magnetocaloric effect for **2a** is $-\Delta S_M$ = 22.7 J kg^{-1} K^{-1}, and $-\Delta S_M$ = 27.7 J kg^{-1} K^{-1}, respectively. These values are close to the experimental one (22.9 J kg^{-1} K^{-1}), which shows the good prediction capability of these relationships.

Theoretical calculations

Density Functional Theory (DFT) was used to support our findings from fitting the experimental magnetic data for the Gd^{III} compounds. The well-known B3LYP functional was used to calculate high-spin (HS) and broken-symmetry (BS) spin states

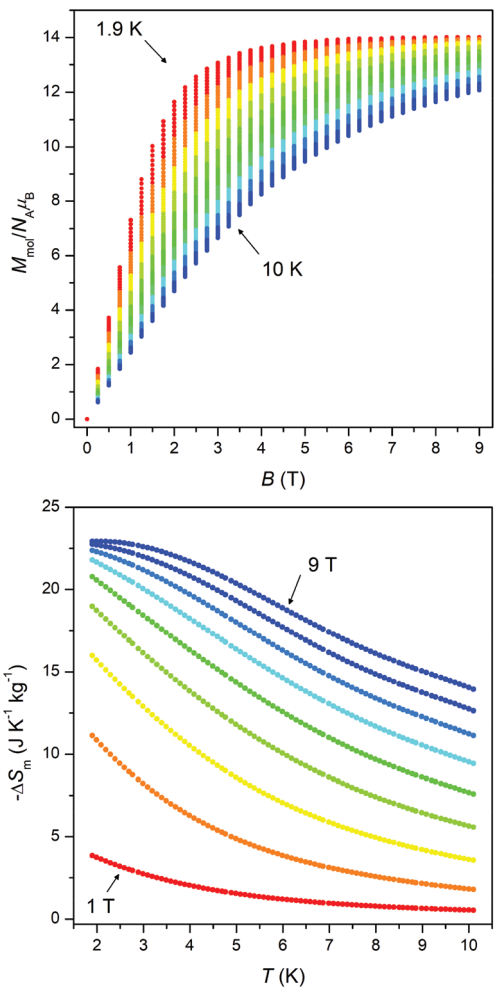

Fig. 6 Top: The densely-measured magnetization data of **2a**. Bottom: The isothermal magnetic entropy change ($-\Delta S_M$) of **2a** calculated using eqn (5).

with ORCA 3.0.3. Then, the energy difference between these states, $\Delta = \varepsilon_{BS} - \varepsilon_{HS}$, was utilized in the calculation of the isotropic exchange parameter J following Ruiz's approach as

$$J = 2\Delta/[(S_1 + S_2)(S_1 + S_2 + 1)] \quad (6)$$

which resulted in $J = -0.18$ cm^{-1} for **1a** and $J = -0.20$ cm^{-1} for **2a**. These values supported the presence of the antiferromagnetic exchange and are in good agreement with parameters derived from the analysis of magnetic data with spin Hamiltonian in eqn (1).

Furthermore, the post-Hartree–Fock CASSCF calculations were employed in order to better understand the magnetic behaviour of Dy^{III} SMM compounds, namely the ferromagnetic interactions which are evident at low temperatures (Fig. 4) and also different relaxation behaviours (Fig. 5). Thus, the CASSCF calculations were performed with MOLCAS 8.0 for dinuclear molecular fragments $[DyLu(3m\text{-}L4)_2(L2)_2(MeOH)_2]$ of **1c** and $[DyLu(3m\text{-}L4)_2(L2)_2(DMF)_2]$ of **2c**, in which one Dy^{III} atom was replaced with a diamagnetic Lu^{III} atom.

Subsequent analysis with the SINGLE_ANISO module of MOLCAS revealed the splitting of the $^6H_{15/2}$ atomic term into eight Kramers doublets (KD). Each Kramers doublet was then analysed with effective spin $S_{eff} = 1/2$, which resulted in effective g-tensor values (g_x, g_y, g_z) – Tables 3 and 4.

Table 3 Energy levels of lowest ligand field multiplets in zero magnetic field derived from CASSCF/DKH2/SINGLE_ANISO calculations for the molecular fragment $[DyLu(3m\text{-}L4)_2(L2)_2(MeOH)_2]$ of **1c** with the respective g-factors derived for each Kramers doublet with effective spin 1/2[a]

E/k (K)	g_x	g_y	g_z	α (°)
0	0.020	0.030	19.60	
225	0.899	1.836	15.52	26.0
296	0.370	2.474	12.23	35.4
376	1.411	4.777	10.17	56.2
438	0.062	1.907	17.07	54.5
461	3.045	6.307	9.61	71.8
553	1.131	2.056	17.43	97.3
768	0.044	0.094	19.71	121.0

[a] α is an angle of g_z of the excited state with respect to g_z of the ground Kramers doublet.

Table 4 Energy levels of lowest ligand field multiplets in zero magnetic field derived from CASSCF/DKH2/SINGLE_ANISO calculations for the molecular fragment $[DyLu(3m\text{-}L4)_2(L2)_2(DMF)_2$ of **2c** with the respective g-factors derived for each Kramers doublet with the effective spin 1/2[a]

E/k (K)	g_x	g_y	g_z	α (°)
0	0.005	0.007	19.53	
223	0.272	0.679	15.92	11.4
280	1.184	2.348	16.37	64.2
329	9.281	6.139	2.735	132
411	0.609	4.166	10.96	84.2
489	1.022	1.557	16.36	76.6
514	1.277	2.171	15.86	60.4
639	0.161	0.363	19.40	123

[a] α is an angle of g_z of the excited state with respect to g_z of the ground Kramers doublet.

Evidently, ground states in **1c** and **2c** possess a very large axial magnetic anisotropy, $g_x = g_y \approx 0$ and $g_z \approx 19.5$–19.6. The first excited states are separated by 225 and 223 K for **1c**, and **2c**, respectively, and both have quite large axial magnetic anisotropy (Tables 3 and 4), but g_x and g_y components are already non-zero. Moreover, the larger deviation of the easy-axis of the g-tensor of the first excited state from the easy-axis of the g-tensor of the ground state is observed for **1c** (α = 26.0° for **1c** and α = 11.4° for **2c**) – (Tables 3 and 4). Next, the plots of the magnetization blocking barrier were constructed for **1c** and **2c** (Fig. 7), where the values of the transition magnetic moments between Kramers levels are shown and this plot suggests that there is a very low probability of the quantum tunnelling of the ground state and that the relaxation through the first excited states is most probable. To summarize, both compounds should be SMMs in the zero static magnetic field and **2c** has predisposition to be a slightly better SMM, because it reveals (i) a better axial type of the magnetic anisotropy of the ground and the first excited states, (ii) a better collinearity of the g-tensors of the first

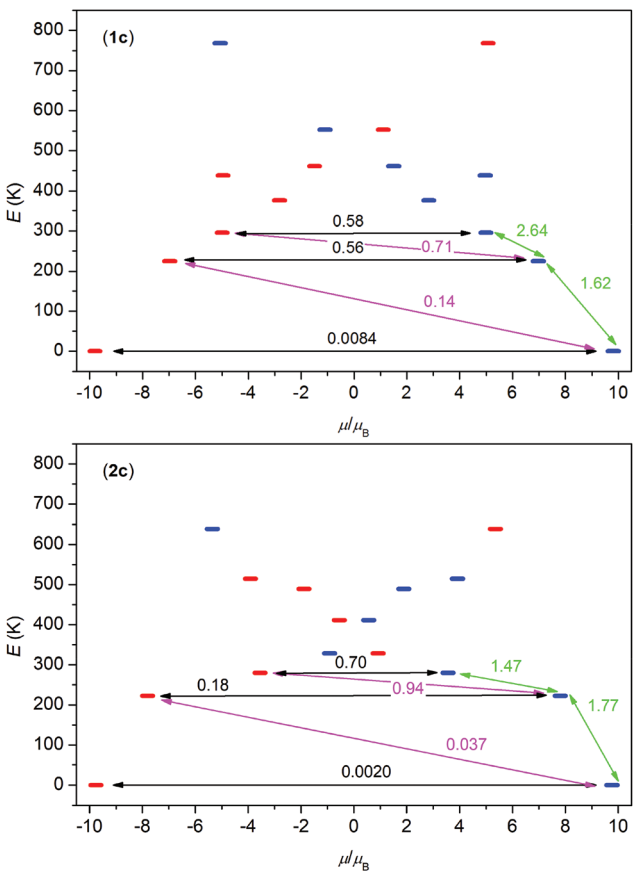

Fig. 7 The *ab initio* computed magnetization blocking barrier for the molecular fragments $[DyLu(3m\text{-}L4)_2(L2)_2(MeOH)_2]$ of **1c** and $[DyLu(3m\text{-}L4)_2(L2)_2(DMF)_2]$ of **2c**. The thick blue/red bars indicate the Kramer's doublets (KDs) as a function of their magnetic moment. Green lines indicate the magnetization reversal mechanism. The magenta lines show the possible pathway of the Orbach process. The black lines represent the presence of QTM/TA-QTM between the connecting pairs.

excited and the ground states. In the next step, the POLY_ANISO module was utilized to calculate the DC magnetic properties of **1c** and **2c** using the data from the SINGLE_ANISO module and the information that Dy atoms are related to each other through inversion symmetry operation. The orientation of the magnetic moments with respect to the Dy···Dy connecting line (angle θ) in these centrosymmetric dinuclear compounds is the crucial factor for observing either antiferromagnetic or ferromagnetic dipole–dipole interactions due to the following relationship

$$E_{\text{dipolar}} = -\frac{\mu_0}{4\pi}\frac{\mu_i\mu_j}{r^3}\left(3\cos^2\theta - 1\right) \quad (7)$$

for the energy of the dipole–dipole interaction.[31]

Consequently, for $\theta < 54.7°$ the ferromagnetic interaction is expected, whereas for $\theta > 54.7°$ the antiferromagnetic interaction is anticipated. Here, we have found that $\theta = 7.6°$ for **1c** and $\theta = 9.3°$ for **2c** (Fig. 8), therefore these findings are in agreement with the observed increase of the effective magnetic moment at low temperatures due to the ferromagnetic dipole–dipole interactions (Fig. 9).

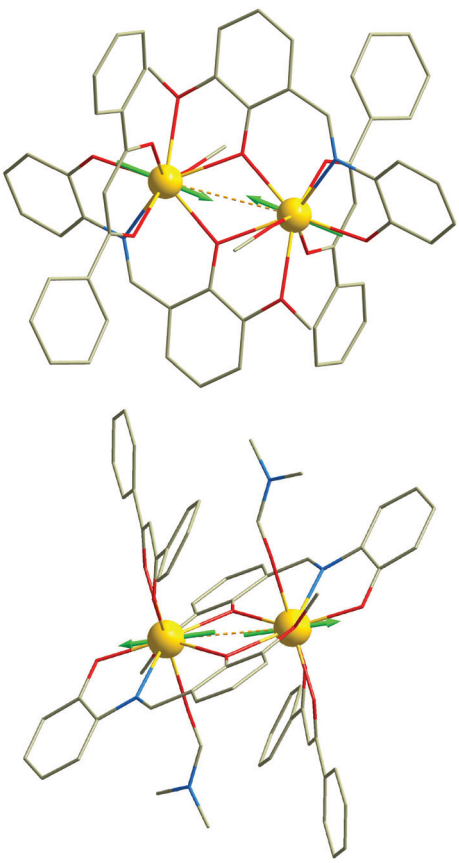

Fig. 8 The *ab initio* computed easy-axes of the ground state for **1c** (top) and for **2c** (bottom). The green arrows show the orientation of the *ab initio* computed orientation of the principal magnetization axes of the ground-state Kramers doublets and dotted lines serve as a guide to eyes to show the connecting line between the Dy atoms.

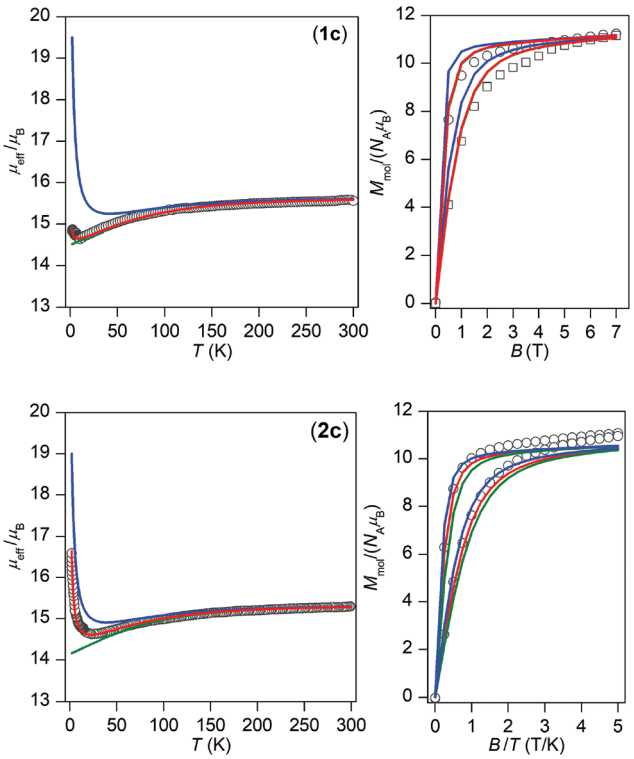

Fig. 9 Magnetic data for Dy^{III} complexes **1c** and **2c**. Temperature dependence of the effective magnetic moment (left) and the isothermal molar magnetizations measured at 2 (○) and 5 (□) K (right). The full lines correspond to the calculated data using module POLY_ANISO scaled with the factor equal to 1.094 for **1c** and 1.048 for **2c**. Green line – calculation without any interactions, blue line – calculation with the dipolar interaction, red line – calculation with the dipolar interaction and additional exchange interaction $J_{exh} = -0.24$ cm^{-1} for **1c** and $J_{exh} = -0.16$ cm^{-1} for **2c** applied, respectively.

This dipolar origin of the ferromagnetic interaction is clearly visible from the comparison of green and blue lines in Fig. 9, where the first green line corresponds to the calculated magnetic properties without dipolar interactions, while the second one comprises the dipolar interactions. In both compounds **1c** and **2c**, a better agreement with the experimental data was achieved by including additional antiferromagnetic exchange coupling $J_{ex} = -0.24$ cm^{-1} for **1c** and $J_{ex} = -0.16$ cm^{-1} for **2c** (red lines in Fig. 9). To summarize, the analysis of magnetic data with the POLYANISO module revealed ferromagnetic dipolar interactions between the Dy^{III} atoms within the dinuclear units accompanied by weak antiferromagnetic superexchange coupling.

Experimental section

Materials

All the purchased chemicals were chemically pure and of analytical reagent grade, and were used without further purification. The preparations of **1a–c** and **2a–c** are very similar and

therefore only the synthesis of **1a** will be exemplified in greater detail.

$[Gd_2^{III}(3m\text{-}L4)_2(L2)_2(MeOH)_2]\cdot 6MeOH$ (1a)

3-Methoxysalicylaldehyde (0.5 mmol, 0.078 g) and 2-aminophenol (0.5 mmol, 0.055 g) were dissolved in MeOH (15 ml) to obtain an orange solution. A solution of the ligand HL2 (0.5 mmol, 0.112 g) in MeOH (15 ml) and $Gd(NO_3)_3\cdot 6H_2O$ (0.5 mmol, 0.226 g) in MeOH (10 ml) were added giving a bright red solution. A solution of Pr_3N (tripropylammine, 1.5 mmol, 0.215 g) in 5 cm^3 MeOH was dropwise added after 10 min of stirring at room temperature. The resulting yellow solution was filtered and left undisturbed to evaporate the solvent at room temperature. Orange prism shaped crystals were formed after 4 days and collected by filtration. Yield: 36%. Anal. calcd for **1a** ($C_{58}H_{44}Gd_2N_2O_{10}\cdot H_2O$, M_{mol} = 1261.52 g mol^{-1}): C, 55.2; H, 3.7; N, 2.2, found: C, 55.1; H, 3.5; N, 2.0; IR mid (in cm^{-1}): ν(O–H) = 3594 (w), $\nu(C–H)_{aromatic}$ = 3056 (w), $\nu(C–H)_{aliphatic}$ = 2938, 2905 (w), ν(C═C), ν(C═N) = 1596, 1549, 1514 (s), ν(C–O) = 1221 (s). TG/DTA data: weight loss of 2.7% found in the 24–136 °C region with the endothermic peak centered at 58 °C (2.8% calcd for 2.5 H_2O).

$[Tb_2^{III}(3m\text{-}L4)_2(L2)_2(MeOH)_2]\cdot 6MeOH$ (1b), $[Dy_2^{III}(3m\text{-}L4)_2(L2)_2(MeOH)_2]\cdot 6MeOH$ (1c)

These compounds were prepared in an identical manner to **1a** by replacing $Gd(NO_3)_3\cdot 6H_2O$ with the corresponding hydrated nitrate salts ($Tb(NO_3)_3\cdot 5H_2O$, 0.5 mmol, 0.219 g – **1b**; $Dy(NO_3)_3\cdot 6H_2O$, 0.5 mmol, 0.230 g – **1c**). Compound **1b**: Yield 45%. Anal. calcd ($C_{58}H_{44}Tb_2N_2O_{10}\cdot 2H_2O$, M_{mol} = 1282.88 g mol^{-1}): C, 54.3; H, 3.8; N, 2.2, found: C, 54.3; H, 3.6; N, 2.1; IR mid (in cm^{-1}): ν(O–H) = 3310 (w), $\nu(C–H)_{aromatic}$ = 3056 (w), $\nu(C–H)_{aliphatic}$ = 2937 (w), ν(C═C), ν(C═N) = 1595, 1550, 1515 (s), ν(C–O) = 1221 (s). TG/DTA data: weight loss of 2.5% found in the 28–142 °C region with the endothermic peak centered at 85 °C (2.8% calcd for 2 H_2O). Compound **1c**: Yield 42%. Anal. calcd ($C_{58}H_{44}Dy_2N_2O_{10}\cdot 2H_2O$, M_{mol} = 1292.05 g mol^{-1}): C, 53.9; H, 3.9; N, 2.2, found: C, 53.6; H, 3.6; N, 2.0; IR mid (in cm^{-1}): ν(O–H) = 3315 (w), $\nu(C–H)_{aromatic}$ = 3056 (w), $\nu(C–H)_{aliphatic}$ = 2937, 2908 (w), ν(C═C), ν(C═N) = 1596, 1549, 1515 (s), ν(C–O) = 1221 (s). TG/DTA data: weight loss of 2.6% found in the 28–134 °C region with the endothermic peak centered at 93 °C (2.8% calcd for 2 H_2O).

$[Gd_2^{III}(3m\text{-}L4)_2(L2)_2(DMF)_2]$ (2a), $[Tb_2^{III}(3m\text{-}L4)_2(L2)_2(DMF)_2]$ (2b), $[Dy_2^{III}(3m\text{-}L4)_2(L2)_2(DMF)_2]$ (2c)

These compounds were prepared following the same procedure in relation to **1a–c**, but instead of MeOH (40 cm^3) as the reaction solvent, a mixture of MeOH (40 cm^3) and DMF (2 cm^3) was used. Compound **2a**: Yield: 44%. Anal. calcd ($C_{58}H_{44}Gd_2N_2O_{10}\cdot 2C_3H_7NO$, M_{mol} = 1389.70 g mol^{-1}): C, 55.3; H, 4.2; N, 4.0, found: C, 55.6; H, 4.2; N, 3.8; IR mid (in cm^{-1}): $\nu(C–H)_{aromatic}$ = 3054 (w), $\nu(C–H)_{aliphatic}$ = 2914 (w), ν(C═O) = 1650 (vs), ν(C═C), ν(C═N) = 1598, 1551, 1513 (s), ν(C–O) = 1218 (s). Compound **2b**: Yield: 52%. Anal. calcd ($C_{58}H_{44}Tb_2N_2O_{10}\cdot 2C_3H_7NO$, M_{mol} = 1393.06 g mol^{-1}): C, 55.1; H, 4.3; N, 4.0, found: C, 54.7; H, 4.2; N, 3.8; IR mid (in cm^{-1}): $\nu(C–H)_{aromatic}$ = 3054 (w), $\nu(C–H)_{aliphatic}$ = 2916 (w), ν(C═O) = 1650 (vs), ν(C═C), ν(C═N) = 1598, 1551, 1512 (s), ν(C–O) = 1218 (s). Compound **2c**: Yield: 50%. Anal. calcd ($C_{58}H_{44}Dy_2N_2O_{10}\cdot 2C_3H_7NO$, M_{mol} = 1402.21 g mol^{-1}): C, 54.8; H, 4.3; N, 4.0, found: C, 54.6; H, 4.3; N, 3.8; IR mid (in cm^{-1}): $\nu(C–H)_{aromatic}$ = 3054 (w), $\nu(C–H)_{aliphatic}$ = 2914 (w), ν(C═O) = 1650 (vs), ν(C═C), ν(C═N) = 1598, 1551, 1513 (s), ν(C–O) = 1218 (s).

Methods

Elemental analyses (C, H, N) were performed on a FLASH 2000 CHNS-O Analyzer (ThermoFisher Scientific). The infrared spectra of the complexes were recorded on a ThermoNicolet NEXUS 670 FT-IR spectrometer using the ATR technique in the range of 4000–400 cm^{-1}. The temperature dependent (T = 1.9–300 K, B = 0.1 T) and field dependent (B = 0–7 T, T = 2 and 4.6 or 5 K) magnetization measurements on polycrystalline samples were performed with a MPMS XL-7 Quantum Design SQUID magnetometer. Experimental data were corrected for the diamagnetism of the constituent atoms.

X-ray diffraction analysis

X-ray measurements on the selected single crystals of **1a–c** and **2b–c** were performed on an Oxford Diffraction Xcalibur™[2] equipped with a Sapphire 2 CCD detector using the Mo-Kα radiation (λ = 0.71073 Å) and Oxford Cryosystems nitrogen gas-flow apparatus. The CrysAlis program package (version 1.171.33.52, Oxford Diffraction) was used for data collection and reduction.[32] X-ray measurement on the single-crystal of **2a** was performed on a Bruker D8 Quest diffractometer equipped with a Photon 100 CMOS detector using the Mo-Kα radiation. Data collection, data reduction, and cell parameter refinements were performed using the Bruker Apex III software package.[33] The molecular structures were solved by direct methods SHELXS-2014 and all non-hydrogen atoms were refined anisotropically on F^2 using the full-matrix least-squares procedure SHELXL-2014.[34] All hydrogen atoms were found in differential Fourier maps and their parameters were refined using the riding model with U_{iso}(H) = 1.2 (CH, CH_2, and OH) or 1.5U_{eq} (CH_3).

The shape of coordination polyhedra was calculated using the program Shape (version 2.1).[24]

Theoretical methods

The DFT calculations were performed with the program ORCA 3.0.3.[35] The hybrid B3LYP functional[36] was used for the calculations of the isotropic exchange constants J for Gd^{III} compounds **1a** and **2a** following Ruiz's approach[37] by comparing the energies of high spin (HS) and broken-symmetry spin (BS) states. The relativistic effects were also included in the calculation with zero order regular approximation (ZORA)[38,39] together with the scalar relativistic contracted version of the basis functions def2-TZVP for Gd, N, and O atoms and def2-SVP for C and H atoms.[40] We also used the chain-of-spheres

approximation to exact exchange (RIJCOSX).[41] The molecular geometries were extracted from the experimental X-ray data.

The post-Hartree–Fock calculations were performed with the MOLCAS 8.0 program package[42] for Dy^{III} compounds **1c** and **2c** with the geometries experimentally determined by X-ray analysis. The active space of the CASSCF calculations[43] comprised nine electrons in seven metal-based f-orbitals, CAS (9,7). The RASSCF method was employed in the CASSCF calculations with the following numbers of multiplets: 21 sextets, 224 quartets and 490 doublets. The spin–orbit coupling based on the atomic mean field approximation (AMFI)[44] was taken into account using RASSI-SO with the following numbers of multiplets: 21 sextets, 128 quartets and 130 doublets. The relativistic effects were treated with the Douglas–Kroll Hamiltonian.[45] The following basis sets were employed: Dy.ANO-RCC-VQZP, Lu.ANO-RCC-VDZ, O.ANO-RCC-VDZ, N.ANO-RCC-VDZ, C.ANO-RCC-MB and H.ANO-RCC-MB.[46] Then, the SINGLE_ANISO module[47] and POLY_ANISO module[48] were used to calculate all relevant information and magnetic data.

Conclusions

In conclusion, six dinuclear lanthanide complexes $[Ln_2(3m\text{-}L4)_2(L2)_2(MeOH)_2]\cdot 6MeOH$ (Ln = Gd – **1a**, Tb – **1b**, and Dy – **1c**) and $[Ln_2(3m\text{-}L4)_2(L2)_2(DMF)_2]$ (Ln = Gd – **2a**, Tb – **2b**, and Dy – **2c**) were prepared and thoroughly characterized. It was revealed that the incorporation of different solvent molecules, *i.e.* MeOH (**1a–c**) and DMF (**2a–c**), into the structures of these compounds affected their magnetic properties considerably. The magnetic coupling between the Gd metal centres in **1a** and **2a** was studied theoretically by the BS-DFT calculations and predicted to be weakly antiferromagnetic in both compounds (in cm^{-1}, $J = -0.18$ **1a**, -0.20, **2a**), and this is in a very good agreement with the results obtained by the spin Hamiltonian fitting of the experimental magnetic data (in cm^{-1}, $J = -0.13$ **1a**, -0.17, **2a**). Both Dy_2 compounds exhibit ferromagnetic interactions of clearly dipolar character as it was revealed by the theoretical analysis using the Lines model. Different strengths of the magnetic interactions in **1c** and **2c** were ascribed to different mutual orientations of the magnetic moments within the Dy_2 dimers. Single molecule magnet behaviour in zero DC field was found in both Dy_2 compounds, but the AC susceptibility measurements revealed the presence of the well-defined maxima only for compound **2c**.

The magnetocaloric effect was investigated on compound **2a** and the experimentally derived value $-\Delta S_M = 22.9$ J kg^{-1} K^{-1} at $T = 2.0$ K and $B = 9$ T is the highest one for the Gd_2 double phenoxo-bridged compounds observed up to now.

Conflicts of interest

There are no conflicts to declare.

Acknowledgements

We acknowledge the financial support from the National Programme of Sustainability I (LO1305) of the Ministry of Education, Youth and Sports of the Czech Republic.

Notes and references

1 G. R. Motson, J. S. Fleming and S. Brooker, *Adv. Inorg. Chem.*, 2004, **55**, 361–432.
2 E. D. Bloch, W. L. Queen and R. Krishna, *Science*, 2012, **335**, 1606.
3 (*a*) M. Bottrill, L. Kwok and N. J. Long, *Chem. Soc. Rev.*, 2006, **35**, 557–571; (*b*) E. Debroye and T. N. Parac-Vogt, *Chem. Soc. Rev.*, 2014, **43**, 8178–8192.
4 (*a*) K. A. Gschneidner and V. K. Pecharsky, *J. Rare Earths*, 2006, **24**, 641–647; (*b*) J. Romero Gómez, R. Ferreiro Garcia, A. de Miguel Catoira and M. Romero Gómez, *Renewable Sustainable Energy Rev.*, 2013, **17**, 74–82.
5 K. Tordrup and K. Molner, *Phys. Rev. A*, 2007, **75**, 022316.
6 J. M. Clemente-Juan, E. Coronado and A. Gaita-Arino, *Chem. Soc. Rev.*, 2012, **41**, 7464–7478.
7 (*a*) R. Sessoli and A. K. Powell, *Coord. Chem. Rev.*, 2009, **253**, 2328–2341; (*b*) L. Sorace, C. Benelli and D. Gatteschi, *Chem. Soc. Rev.*, 2011, **40**, 3092–3104; (*c*) D. N. Woodruff, R. E. P. Winpenny and R. A. Layfield, *Chem. Rev.*, 2013, **113**, 5110–5148; (*d*) F. Habib and M. Murugesu, *Chem. Soc. Rev.*, 2013, **42**, 3278–3288.
8 D. N. Woodruff, R. E. P. Winpenny and R. A. Layfield, *Chem. Rev.*, 2013, **113**, 5110–5148.
9 (*a*) D. Aravena and E. Ruiz, *Inorg. Chem.*, 2013, **52**, 13770–13778; (*b*) S. K. Singh, T. Gupta and G. Rajaraman, *Inorg. Chem.*, 2014, **53**, 10835–10845; (*c*) S. Gómez-Coca, D. Aravena, R. Morales and E. Ruiz, *Coord. Chem. Rev.*, 2015, **289–290**, 379–392.
10 (*a*) K. R. Meihaus, J. D. Rinehart and J. R. Long, *Inorg. Chem.*, 2011, **50**, 8484–8489; (*b*) S. N. Konig, N. F. Chilton, C. Maichle-Mossmer, E. M. Pineda, T. Pugh, R. Anwander and R. A. Layfield, *Dalton Trans.*, 2014, **43**, 3035–3038; (*c*) L. Li, S. Liu, H. Li, W. Shi and P. Cheng, *Chem. Commun.*, 2015, **51**, 10933–10936.
11 (*a*) V. S. Mironov, Y. G. Galyametdinov, A. Ceulemans, C. Gorller-Walrand and K. Binnemans, *Chem. Phys. Lett.*, 2001, **345**, 132–140; (*b*) V. S. Mironov, Y. G. Galyametdinov, A. Ceulemans, C. Gorller-Walrand and K. Binnermans, *J. Chem. Phys.*, 2002, **116**, 4673–4685; (*c*) J. D. Rinehart and J. R. Long, *Chem. Sci.*, 2011, **3**, 2078–2085.
12 N. F. Chilton, D. Collison, J. L. McInnes, R. E. P. Winpenny and A. Soncini, *Nat. Commun.*, 2013, **4**, 2551–2557.
13 (*a*) Y. Guo, G. Xu, W. Wernsdorfer, L. Ungur, Y. Guo, J. Tang, H. Zhang, L. F. Chilbotaru and A. K. Powell, *J. Am. Chem. Soc.*, 2011, **133**, 11948–11951; (*b*) F. Habib, P.-H. Lin, J. Long, I. Korobkov, W. Wernsdorfer and M. Murugesu, *J. Am. Chem. Soc.*, 2011, **133**, 8830–8833; (*c*) T. Fukuda, K. Matsumura and N. Ishikawa, *J. Phys. Chem. A*, 2013, **117**,

10447–10454; (*d*) K. Katoh, R. Asano, A. Miura, Y. Horii, T. Morita, B. K. Breedlove and M. Yamashita, *Dalton Trans.*, 2014, **43**, 7716–7725.

14 (*a*) Y.-N. Guo, G.-F. Xu, Y. Guo and J. Tang, *Dalton Trans.*, 2011, **40**, 9953–9963; (*b*) P. Zhang, Y.-N. Guo and J. Tang, *Coord. Chem. Rev.*, 2013, **257**, 1728–1763.

15 (*a*) P.-H. Lin, T. J. Burchell, L. Ungur, L. F. Chibotaru, W. Wernsdorfer and M. Murugesu, *Angew. Chem., Int. Ed.*, 2009, **48**, 9489–9492; (*b*) Y. Ma, G. F. Xu, X. Yang, L. C. Li, J. Tang, S. P. Yan, P. Cheng and D. Z. Liao, *Chem. Commun.*, 2010, **46**, 8264–8266; (*c*) F. Tuna, C. A. Smith, M. Bodensteiner, L. Ungur, L. F. Chibotaru, E. J. L. McInnes, R. E. P. Winpenny, D. Collison and R. A. Layfield, *Angew. Chem., Int. Ed.*, 2012, **51**, 6976–6780; (*d*) R. J. Blagg, L. Ungur, F. Tuna, J. Speak, P. Comar, D. Collison, W. Wernsdorfer, E. J. L. McInnes, L. F. Chibotaru and R. E. P. Winpenny, *Nat. Commun.*, 2013, **5**, 673–679; (*e*) J. Liu, Y.-C. Chen, J.-L. Liu, V. Vieru, L. Ungur, J.-H. Jia, L. F. Chibotaru, Y. Lan, W. Wernsdorfer, S. Gao, X.-M. Chen and M.-L. Tong, *J. Am. Chem. Soc.*, 2016, **138**, 5441–5450; (*f*) C. A. P. Goodwin, F. Ortu, D. Reta, N. F. Chilton and D. P. Mills, *Nature*, 2017, **548**, 439–442.

16 N. F. Chilton, S. K. Langley, B. Moubaraki, A. Soncini, S. R. Batten and K. S. Murray, *Chem. Sci.*, 2013, **4**, 1719–1730.

17 (*a*) P.-H. Lin, T. J. Burchell, R. Clérac and M. Murugesu, *Angew. Chem., Int. Ed.*, 2008, **47**, 8848–8851; (*b*) Y.-N. Guo, X.-H. Chen, S. Xue and J. Tang, *Inorg. Chem.*, 2011, **50**, 9705–9713; (*c*) J. Long, F. Habib, P. H. Lin, I. Korobkov, G. Enright, L. Ungur, W. Wernsdorfer, L. F. Chibotaru and M. Murugesu, *J. Am. Chem. Soc.*, 2011, **133**, 5319–5328; (*d*) L. Zou, L. Zhao, P. Chen, Y.-N. Guo, Y.-H. Li and J. Tang, *Dalton Trans.*, 2012, **41**, 2966–2971; (*e*) P. Zhang, L. Zhang, S.-Y. Lin, S. Xue and J. Tang, *Inorg. Chem.*, 2013, **52**, 4587–4592; (*f*) N. C. Anastasiadis, D. A. Kalofolias, A. Philippidis, S. Tzani, C. P. Raptopoulou, V. Psycharis, C. J. Milios, A. Escuer and S. P. Perlepes, *Dalton Trans.*, 2015, **44**, 10200–10209.

18 (*a*) M. Evangelisti, O. Roubeau, E. Palacious, A. Camón, T. N. Hooper, E. K. Brechin and J. J. Alonso, *Angew. Chem., Int. Ed.*, 2011, **50**, 6606–6609; (*b*) F.-S. Guo, J.-D. Leng, J.-L. Liu, Z.-S. Meng and M.-L. Tong, *Inorg. Chem.*, 2012, **51**, 405–413; (*c*) J.-M. Jia, S.-J. Liu, Y. Cui, S.-D. Han, T.-L. Hu and X.-H. Bu, *Cryst. Growth Des.*, 2013, **13**, 4331–4334; (*d*) S. Biswas, A. Adhikary, S. Goswami and S. Konar, *Dalton Trans.*, 2013, **42**, 13331–13334; (*e*) Y.-C. Chen, F.-S. Guo, Y.-Z. Zheng, J.-L. Liu, J.-D. Leng, R. Tarasenko, M. Orendáč, J. Prokleška, V. Sechovský and M.-L. Tong, *Chem. – Eur. J.*, 2013, **19**, 13504–13510; (*f*) Y. Meng, Y.-C. Chen, Z.-M. Zhang, Z.-J. Lin and M.-L. Tong, *Inorg. Chem.*, 2014, **53**, 9052–9057; (*g*) Y. Yang, Q.-C. Zhang, Y.-Y. Pan, L.-S. Long and L.-S. Zheng, *Chem. Commun.*, 2015, **51**, 7317–7320.

19 J. W. Sharples and D. Collison, *Polyhedron*, 2013, **54**, 91–103.

20 K. Zhang, D. Liu, V. Vieru, L. Hou, B. Cui, F.-S. Guo, L. F. Chibotaru and Y.-Y. Wang, *Dalton Trans.*, 2017, **46**, 638–642.

21 (*a*) J.-F. Dong, L. Li, Z.-Z. Ji, H. Cui and D.-Q. Wang, *Acta Crystallogr., Sect. E: Struct. Rep. Online*, 2007, **63**, 1578; (*b*) I. Nemec, M. Machata, R. Herchel, R. Boča and Z. Trávníček, *Dalton Trans.*, 2012, **41**, 14603–14610; (*c*) S. Bag, P. K. Bhaumik, S. Jana, M. Das, P. Bhowmik and S. Chattopadhyay, *Polyhedron*, 2013, **66**, 229–237; (*d*) M. Hasanzadeh, M. Salehi, M. Kubicki, S. M. Shahcheragh, G. Dutkiewicz, M. Pyziak and A. Khaleghian, *Transition Met. Chem.*, 2014, **39**, 623–632.

22 (*a*) K. C. Mondal, G. E. Kostakis, Y. Lan, W. Wernsdorfer, C. E. Anson and A. K. Powell, *Inorg. Chem.*, 2011, **50**, 11604–11610; (*b*) K. C. Mondal, A. Sundt, Y. Lan, G. E. Kostakis, O. Waldmann, L. Ungur, L. F. Chibotaru, C. E. Anson and A. K. Powell, *Angew. Chem., Int. Ed.*, 2012, **51**, 7550–7554; (*c*) H. Ke, L. Zhao, Y. Guo and J. Tang, *Inorg. Chem.*, 2012, **51**, 2699–2705; (*d*) K. C. Mondal, G. E. Kostakis, Y. Lan and A. K. Powell, *Polyhedron*, 2013, **66**, 268–273; (*e*) S. Saha, S. Pal, C. J. Gómez-García, J. M. Clemente-Juan, K. Harms and H. P. Nayek, *Polyhedron*, 2014, **74**, 1–5; (*f*) K. Griffiths, C. W. D. Gallop, A. Abdul-Sada, A. Vargas, O. Navarro and G. E. Kostakis, *Chem. – Eur. J.*, 2015, **21**, 6358–6361; (*g*) H. Ke, W. Zhu, S. Zhang, G. Xie and S. Chen, *Polyhedron*, 2015, **87**, 109–116; (*h*) W.-W. Kuang, C.-Y. Shao and P.-P. Yang, *J. Coord. Chem.*, 2015, **68**, 1412–1422; (*i*) H. Ke, S. Zhang, W. Zhu, G. Xie and S. Chen, *J. Coord. Chem.*, 2015, **68**, 808–822.

23 R. Kannappan, D. M. Tooke, A. L. Spek and J. Reedijk, *Inorg. Chim. Acta*, 2006, **359**, 334–338.

24 (*a*) M. Llunell, D. Casanova, J. Cicera, P. Alemany and S. Alvarez, *SHAPE, Version 2.1*, Barcelona, Spain, 2013; (*b*) S. Alvarez, *Dalton Trans.*, 2005, 2209–2233; (*c*) D. Casanova, P. Alemany, J. M. Bofill and S. Alvarez, *Chem. – Eur. J.*, 2003, **9**, 1281–1295; (*d*) A. Ruiz-Martínez, D. Casanova and S. Alvarez, *Chem. – Eur. J.*, 2008, **14**, 1291–1303; (*e*) A. Ruiz-Martínez, D. Casanova and S. Alvarez, *Dalton Trans.*, 2008, 2583–2591.

25 (*a*) P.-H. Lin, W.-B. Sun, M.-F. Yu, G.-M. Li, P.-F. Yan and M. Murugesu, *Chem. Commun.*, 2011, **47**, 10993–10995; (*b*) F. Gao, Y.-Y. Li, C.-M. Liu, Y.-Z. Li and J.-L. Zuo, *Dalton Trans.*, 2013, **42**, 11043–11046; (*c*) J. Zhu, H.-F. Song, P.-F. Yan, G.-F. Hou and G.-M. Li, *CrystEngComm*, 2013, **15**, 1747–1752; (*d*) H. Wang, C. Liu, T. Liu, S. Zeng, W. Cao, O. Ma, C. Duan, J. Dou and J. Jiang, *Dalton Trans.*, 2013, **42**, 15355–15360; (*e*) A.-J. Hutchings, F. Habib, R. J. Holmberg, I. Korobkov and M. Murugesu, *Inorg. Chem.*, 2014, **53**, 2102–2112; (*f*) E. Moreno Pineda, N. F. Chilton, R. Marx, M. Dorfel, D. O. Sells, P. Neugebauer, S.-D. Jiang, D. Colison, J. van Slageren, E. J. C. McInnes and R. E. P. Winpenny, *Nat. Commun.*, 2014, **5**, 5243–5249; (*g*) F. Gao, X.-M. Zhang, L. Cui, K. Deng, Q.-D. Zeng and J.-L. Zuo, *Sci. Rep.*, 2014, **4**, 5928.

26 The standard deviations were calculated as $\sigma_i = (P_{ii}^{-1} \cdot S/(N-k))^{-1/2}$, where $P_{ij} = \sum(\delta\mu_n/\delta a_i \cdot \delta\mu_n/\delta a_j)$ and $S = \sum(\mu_n - \mu_n^{exp})^2$ with $n = 1$ to N; a_i and a_j are the fitted parameters, N is the number of the experimental points (sum of temperature and field dependent data), μ_n and μ_n^{exp} are the calculated

and experimental effective magnetic moments for the given temperature and magnetic field. The σ_i was then multiplied by Student's $t_{95\%}$ to provide confidence limits with 95% probabilities listed in the text.

27 (*a*) X. Mei, X. Wang, J. Wang, Y. Ma, L. Li and D. Liao, *New J. Chem.*, 2013, **37**, 3620–3626; (*b*) F. Yang, Q. Zhou, G. Zeng, G. Li, L. Gao, Z. Shi and S. Feng, *Dalton Trans.*, 2014, **43**, 1238–1245; (*c*) W. M. Wang, Y. H. Ren, S. Wang, C. F. Zhang, Z. L. Wu, H. Zhang and M. Fang, *Inorg. Chim. Acta*, 2016, **453**, 452–456; (*d*) H.-R. Tu, W.-B. Sun, H.-F. Li, P. Chen, Y.-M. Tian, W.-Y. Zhang, Y.-Q. Zhang and P.-F. Yan, *Inorg. Chem. Front.*, 2017, **4**, 499–508; (*e*) W.-M. Wang, H.-H. Liu, L.-T. He, X.-R. Han, Z.-L. Wu, Y.-G. Ran, J.-Y. Zou and M. Fang, *Polyhedron*, 2017, **133**, 119–124.

28 A. M. Tishin and Y. I. Spichkin, *The Magnetocaloric Effect and its Applications*, IOP Publishing Ltd, 2003.

29 (*a*) W. M. Wang, H. X. Zhang, S. Y. Wang, H. Y. Shen, H. L. Gao, J. Z. Cui and B. Zhao, *Inorg. Chem.*, 2015, **54**, 10610–10622; (*b*) H. Y. Shen, W. M. Wang, Y.-X. Bi, H.-L. Gao, S. Liu and J. Z. Cui, *Dalton Trans.*, 2015, **44**, 18893–18901; (*c*) S.-Y. Wang, W.-M. Wang, H. X. Zhang, S. H.-Y. Shen, L. Jiang, J.-Z. Cui and H.-L. Gao, *Dalton Trans.*, 2016, **42**, 3362–3371.

30 R. Herchel, K. Kotrle and Z. Trávníček, *RSC Adv.*, 2017, **7**, 30763–30769.

31 J.-D. Leng, J.-L. Liu, W.-Q. Lin, S. Gómez-Coca, D. Aravena, E. Ruiz and M.-L. Tong, *Chem. Commun.*, 2013, **49**, 9341–9343.

32 *CrysAlis software package, Version 1.171.33.52*, Agilent, Technologies, Yarnton, England.

33 *Bruker. Apex3*, Bruker AXS Inc., Madison, Wisconsin, USA, 2015.

34 G. M. Sheldrick, *Acta Crystallogr., Sect. C: Cryst. Struct. Commun.*, 2015, **71**, 3–8.

35 F. Neese, *Wiley Interdiscip. Rev.: Comput. Mol. Sci.*, 2012, **2**, 73–78.

36 (*a*) C. Lee, W. Yang and R. G. Parr, *Phys. Rev. B: Condens. Matter*, 1988, **37**, 785–789; (*b*) A. D. Becke, *J. Chem. Phys.*, 1993, **98**, 1372–1377; (*c*) A. D. Becke, *J. Chem. Phys.*, 1993, **98**, 5648–5652; (*d*) P. L. Stephens, F. J. Devlin, C. F. Chabalowski and M. J. Frisch, *J. Phys. Chem.*, 1994, **98**, 11623–11627.

37 (*a*) E. Ruiz, J. Cano, S. Alvarez and P. Alemany, *J. Comput. Chem.*, 1999, **20**, 1391–1400; (*b*) E. Ruiz, A. Rodríguez-Fortea, J. Cano, S. Alvarez and P. Alemany, *J. Comput. Chem.*, 2003, **24**, 982–989.

38 E. V. van Lenthe, E. J. Baerends and J. G. Snijders, *J. Chem. Phys.*, 1993, **99**, 4597–4610.

39 C. van Wüllen, *J. Chem. Phys.*, 1998, **109**, 392–399.

40 D. A. Pantazis, X.-Y. Chen, C. R. Landis and F. Neese, *J. Chem. Theory Comput.*, 2008, **4**, 908–919.

41 (*a*) F. Neese, F. Wennmohs, A. Hansen and U. Becker, *Chem. Phys.*, 2009, **356**, 98; (*b*) R. Izsak and F. Neese, *J. Chem. Phys.*, 2011, **135**, 144105.

42 (*a*) F. Aquilante, L. De Vico, N. Ferré, G. Ghigo, P. Å. Malmqvist, P. Neogrády, T. B. Pedersen, M. Pitoňák, M. Reiher, B. O. Roos, L. Serrano-Andrés, M. Urban, V. Veryazov and R. Lindh, *J. Comput. Chem.*, 2010, **31**, 224–247; (*b*) J. A. Duncan, *J. Am. Chem. Soc.*, 2009, **131**, 2416; (*c*) G. Karlström, R. Lindh, P. Å. Malmqvist, B. O. Roos, U. Ryde, V. Veryazov, P.-O. Widmark, M. Cossi, B. Schimmelpfennig, P. Neogrády and L. Seijo, *Comput. Mater. Sci.*, 2003, **28**, 222–239; (*d*) V. Veryazov, P.-O. Widmark, L. Serrano-Andres, R. Lindh and B. O. Roos, *Int. J. Quantum Chem.*, 2004, **100**, 626–635.

43 P. Å. Malmqvist, B. O. Roos and B. Schimmelpfennig, *Chem. Phys. Lett.*, 2002, **357**, 230–240.

44 (*a*) B. A. Hess, C. M. Marian, U. Wahlgren and O. Gropen, *Chem. Phys. Lett.*, 1996, **251**, 365–371; (*b*) B. Schimmelpfennig, *AMFI, an atomic mean-field spin-orbit integral program*, Stockholm University, 1996.

45 (*a*) N. Douglas and N. M. Kroll, *Ann. Phys.*, 1974, **82**, 89–155; (*b*) B. A. Hess, *Phys. Rev. A*, 1986, **33**, 3742–3748.

46 (*a*) B. O. Roos, R. Lindh, P. Å. Malmqvist, V. Veryazov and P.-O. Widmark, *J. Phys. Chem. A*, 2008, **112**, 11431–11435; (*b*) B. O. Roos, R. Lindh, P. Å. Malmqvist, V. Veryazov and P.-O. Widmark, *Chem. Phys. Lett.*, 2005, **409**, 295–299.

47 (*a*) L. F. Chibotaru, L. Ungur and A. Soncini, *Angew. Chem., Int. Ed.*, 2008, **47**, 4126–4129; (*b*) L. F. Chibotaru, L. Ungur, C. Aronica, H. Elmoll, G. Pillet and D. Luneau, *J. Am. Chem. Soc.*, 2008, **130**, 12445–12455; (*c*) L. F. Chibotaru and L. Ungur, *J. Chem. Phys.*, 2012, **137**, 064112; (*d*) L. Ungur, M. Thewissen, J.-P. Costes, W. Wernsdorfer and L. F. Chibotaru, *Inorg. Chem.*, 2013, **52**, 6328–6337.

48 L. F. Chibotaru, L. Ungur, C. Aronica, H. Elmoll, G. Pilet and D. Luneau, *J. Am. Chem. Soc.*, 2008, **130**, 12445–12455.